A Low-Profile Wideband Hybrid Metasurface Antenna Array for 5G and WiFi Systems

Nian-Sheng Nie, *Student Member, IEEE*, Xue-Song Yang, *Member, IEEE*, Zhi Ning Chen, *Fellow, IEEE*, and Bing-Zhong Wang, *Senior Member, IEEE*

***Abstract*— A hybrid metasurface (HMS) is proposed to form a low-profile wideband antenna array. The antenna element is an array of 4 × 4 square metal patches and fed by a 50 Ω microstrip line through an H-shaped coupling slot on the ground plane. Only are the edge patches of HMS antenna element grounded by shorting pins for the suppression of surface waves and cross-polarization levels as well as the enhancement of the gain. With the HMS antenna element, a compact 2 × 2 array with an overall size of $1.58\lambda_0 \times 1.58\lambda_0 \times 0.068\lambda_0$ (λ_0 is the free-space wavelength at 5.0 GHz) is designed, where the adjacent elements share the edge patches of the elements. The measurement shows the impedance bandwidth of 28% (4.41–5.85 GHz) for $|S_{11}| \leq -10$ dB is obtained, and the boresight gain is greater than 8.4 dBi across the operating band, covering both fifth-generation (5G) sub 6 GHz and WiFi bands.**

***Index Terms*— Antenna array, broadband antenna, hybrid metasurface (HMS), low profile, wide bandwidth.**

I. Introduction

WHEN the fifth-generation (5G) communication system is coming soon, new antenna design is on great demand for the new wireless applications, such as intelligent transportation system, multimedia devices, and advanced mobile systems [1]–[3]. Wideband high-gain patch antennas for 5G sub 6 GHz and WiFi systems have attracted numerous research interest due to their merits of low profile and low cost. However, a conventional microstrip patch antenna suffers from the inherent limitation of narrow operating bandwidth caused by its high quality factor. Many techniques have been developed to increase the impedance bandwidth, typically adopting the stacked patches [4], parasitic resonators [5], and capacitive coupling feeding [6], [7]. However, it is still difficult to widen the bandwidth of low-profile antenna because majority of the wideband designs are based on the quality-factor reduction using a thick substrate or substrate with low dielectric constant or both.

Manuscript received May 3, 2019; revised July 12, 2019; accepted August 30, 2019. Date of publication September 16, 2019; date of current version February 3, 2020. This work was supported by the National Natural Science Foundation of China under Grant 61271027 and Grant 61731005. *(Corresponding author: Xue-Song Yang.)*

N.-S. Nie, X.-S. Yang, and B.-Z. Wang are with the School of Physics, University of Electronic Science and Technology of China, Chengdu 610054, China (e-mail: nieniansheng@126.com; xsyang@uestc.edu.cn).

Z. N. Chen is with the Department of Electrical and Computer Engineering, National University of Singapore, Singapore 117583.

Color versions of one or more of the figures in this article are available online at http://ieeexplore.ieee.org.

Digital Object Identifier 10.1109/TAP.2019.2940367

As an alternative, the antennas loaded with metasurface (MS) [8]–[14] have been proposed to enhance the operating bandwidth and radiation performance of the low-profile antennas. For example, bandwidths of 20% and 23.4% were achieved by stacking an MS above the radiating patches, respectively [8], [9]. In [10], a capacitor-loaded MS was applied to the monopole antennas, achieving an impedance bandwidth of 15% and a gain higher than 6.67 dBi. In [11], an MS was also applied to a dipole antenna for improving the radiation performance, achieving a higher gain of over 8.5 dBi.

Furthermore, the MS antenna in which the MS directly functions as a radiator rather than a reflector or loading of an antenna has been proposed for wideband and low-profile antenna design [15], [16]. Two operating modes with identical radiation performance were well excited by a slot simultaneously over a bandwidth of more than 20%. The rich dispersion characteristics and operating modes of the composite right/left-handed (CRLH) metamaterial structures were analyzed. Moreover, the source-free characteristic mode analysis (CMA) has also been proposed to guide the design of wideband MS antennas [17], [18].

On the other hand, a small interelement spacing is required in an antenna array configuration for suppressing grating lobes, and it is also a key consideration for wideband multiple-input multiple-output (MIMO) antenna systems. Therefore, the low-profile wideband array elements with smaller radiating apertures of the MS antennas rather than the dimensions of $0.73\lambda_0 \times 0.73\lambda_0$ (λ_0 is the free space wavelength) in [15] and [16] are more suitable for wideband antenna array and MIMO systems.

Inspired by the hybrid high impedance surface (HHIS) [19], [20], a hybrid metasurface (HMS) antenna is proposed to form a low-profile wideband antenna array for 5G and WiFi applications. The HMS antenna consists of a 4 × 4 square-metal-patch array, and only the outermost patches are connected to the ground plane by shorting pins, while the internal patches are not shorted. With the shorting pins, surface waves are depressed, and high gain and low cross-polarization levels are achieved. Furthermore, a compact 2 × 2 antenna array is designed by sharing the adjacent shorted patches between the square-metal-patch arrays, and the impedance bandwidth is enhanced by exciting an additional lower frequency resonance. All the numerical simulations are carried out by the full-wave EM simulation software CST Microwave Studio [21].

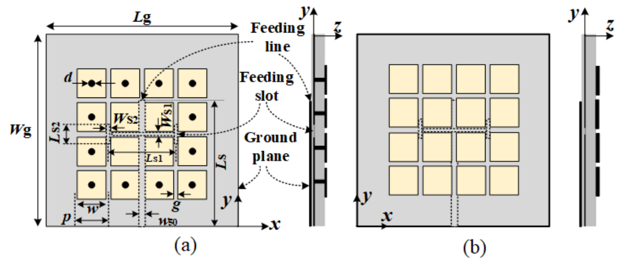

Fig. 1. (a) Proposed HMS in this work. (b) CMS antenna. ($L_g = Wg = 60$, $d = 0.6$, $w = 9$, $g = 1$, $p = 10$, $Ws_1 = 2.4$, $Ls_1 = 20$, $Ws_2 = 2.2$, $Ls_2 = 6$, $w_{50} = 1.85$, and $Ls = 39$. unit: mm).

II. Design of Hybrid Metasurface Antenna

The geometrical configuration of the proposed antenna is shown in Fig. 1(a). The antenna is composed of two layers: a radiating layer and a feeding layer, which are designed on a piece of 3.15 and 0.813 mm-thick F_4BTM substrates ($\varepsilon_r = 3.38$, tan $\delta = 0.0027$ at 10 GHz), respectively. The HMS antenna consists of a 4 × 4 array of square metal patches etched on the top surface of the upper layer, a 50 Ω microstrip feeding line placed on the bottom surface of the lower layer, and a ground plane with an H-shaped coupling slot in the middle of the two substrates. The HMS antenna is similar to the conventional metasurface (CMS) antenna, and the difference between them is that the outermost patches of the HMS are shorted to the ground plane by metal vias, while all the patches of the CMS are not shorted.

The HMS antenna can also be regarded as a grid-slotted patch (GSP) antenna proposed in [16]. Therefore, the transmission-line model is also applicable to the mode analysis of the HMS antenna. The equations for calculating the resonant frequencies of the dual modes are given as follows [15], [16]:

$$\varepsilon_{re} = \frac{\varepsilon_r + 1}{2} + \frac{\varepsilon_r - 1}{2}(1 + 12h/W_p)^{-0.5} \quad (1)$$

$$\frac{\Delta L}{h} = 0.412\frac{(\varepsilon_{re} + 0.3)(W_p/h + 0.262)}{(\varepsilon_{re} - 0.258)(W_p/h + 0.813)} \quad (2)$$

$$\beta_e = 2\pi f\sqrt{\varepsilon_{re}}/c \quad (3)$$

$$4\beta_u p_x/\pi = 1 - 2\beta_e \Delta L/\pi \ \text{TM}_{10} \text{ mode} \quad (4)$$

$$2\beta_u p_x/\pi = 1 - 2\beta_e \Delta L/\pi \ \text{TM}_{20} \text{ mode} \quad (5)$$

where β_u is the propagation constant of the capacitor-loaded patch unit cell, β_e is the propagation constant in the effective extended region with a length of ΔL, f is the operating frequency, and c is the free-space light velocity.

Fig. 2 shows the simulated dispersion diagram of the unit cell with the curves of (4) and (5) for determining the resonant frequencies of TM_{10} and TM_{20} modes. It can be seen that the predicted resonant frequencies of the dual modes based on the transmission-line model are 5.01 and 5.65 GHz.

Fig. 3 shows the simulated reflection coefficient and boresight gain of the HMS antenna. There are two resonant dips at 5.25 and 5.70 GHz. According to the calculated resonant frequencies for TM_{10} and TM_{20} modes, the simulated resonance at the higher frequency is close to the predicted one but that at the lower frequency slightly moves to higher frequency. The reason for the frequency shift is that the effective shunt inductance in the outermost patches is decreased due to the connection of the metal vias to ground. For the HMS antenna, an 18.01% (4.96–5.94 GHz) bandwidth for $|S_{11}| \leq -10$ dB is achieved due to the closely spaced dual modes. Besides, a boresight gain more than 8 dBi is achieved over the band.

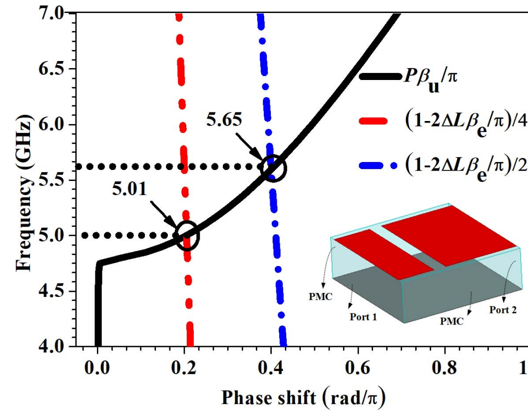

Fig. 2. Dispersion diagram of the series-capacitor-loaded patch unit cell.

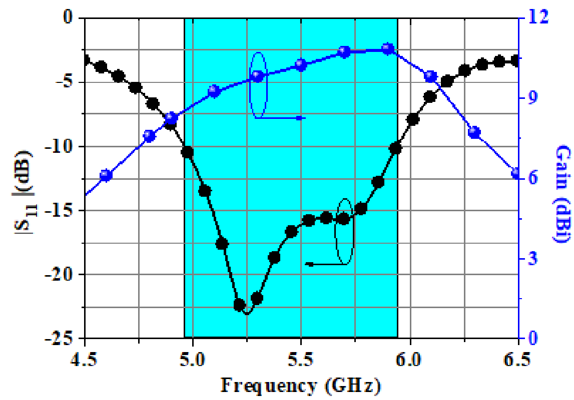

Fig. 3. Simulated reflection coefficient and boresight gain of the HMS antenna.

Figs. 4(a) and 5(a) show the E-field distributions on the plane z = 0.5 mm at the resonant valleys of 5.25 and 5.7 GHz, respectively. It is found that the E-field distributions at the two resonant frequencies of the HMS antenna are similar to the TM_{10} and TM_{20} modes of a conventional patch antenna, but the radiation is from the gaps between the subwavelength square patches, different from a microstrip patch antenna.

Since the dominant surface waves launched in the grounded substrate are along the E-plane of the CMS antenna across the operating band [22], the antenna performance can be improved by depressing the surface waves. The outermost patch array of the HMS antenna can be a 1-D grounded high impedance surface (HIS) for restricting the flow of surface waves, and the dispersion diagram of the mushroom unit cell is calculated as shown in Fig. 6. It can be seen that there exists a complete band gap in a frequency range of 4.2–5.85 GHz. Therefore, the surface waves are blocked by the outermost patches of the HMS antenna. Besides, the simulated model of the mushroom unit cell is depicted in the inset of Fig. 6, and the dimensions of the mushroom unit cell are kept the same as the square patch depicted in Fig. 1(a).

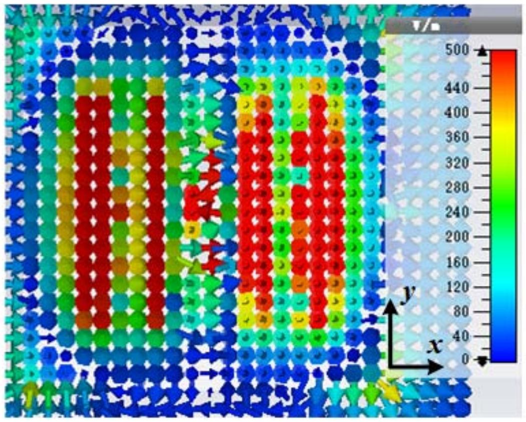

(a)

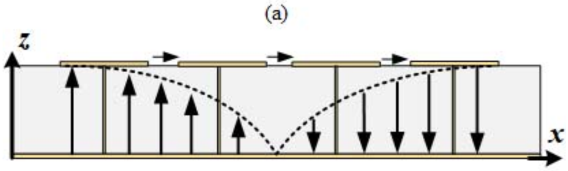

(b)

Fig. 4. TM_{10} mode. (a) Simulated E-field distribution on z = 0.5 mm plane at 5.25 GHz. (b) Sketch of the operation mechanism.

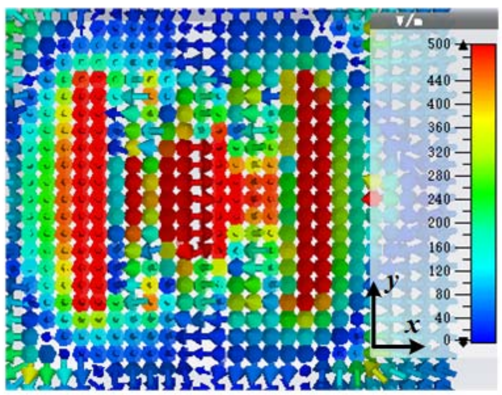

(a)

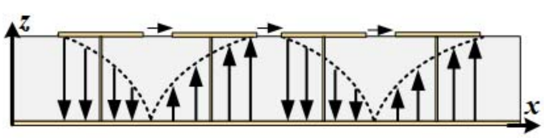

(b)

Fig. 5. TM_{20} mode. (a) Simulated E-field distribution on z = 0.5 mm plane at 5.7 GHz. (b) Sketch of the operation mechanism.

Furthermore, Fig. 7 shows the simulated magnitude current distributions on the ground of the HMS and CMS antennas at 5.5 GHz. The current on the ground edge of the HMS antenna is weaker than that of the CMS antenna because the vias inserted into the outermost patches reduce the flow of surface waves. The simulated boresight gains and cross-polarization levels are given in Fig. 8. It is observed that compared with the CMS antenna, the proposed antenna is with the improved boresight gain by more than 0.5 dB and the reduced cross-polarization levels by more than 60 dB across the frequency band of 5.0–5.9 GHz.

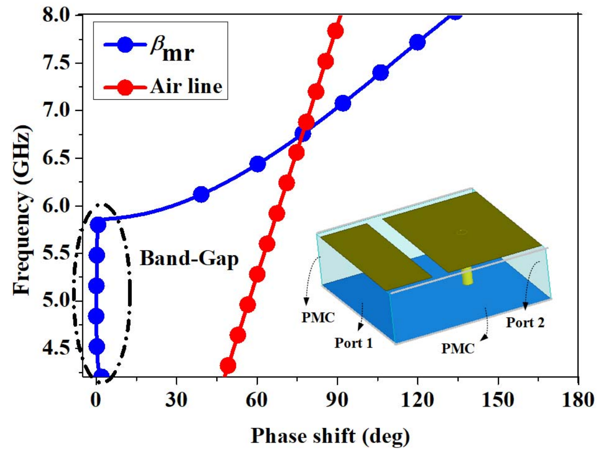

Fig. 6. Simulated dispersion diagram of the mushroom unit cell.

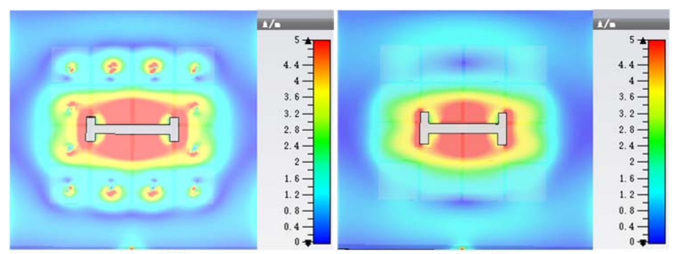

(a) (b)

Fig. 7. Simulated current magnitude distribution on the ground at 5.5 GHz. (a) Proposed HMS antenna in this work. (b) CMS antenna.

III. Antenna Array Design

Based on the proposed HMS antenna design in Section II, a 2 × 2 antenna array is designed and investigated as shown in Fig. 9. The dimensions of the array element remain the same as those in Fig. 1(a), but the adjacent elements share the grounded patch cells. The central distance between two adjacent elements is $d = 0.5\lambda_0$ (λ_0 is the free-space wavelength at 5.0 GHz), and the corresponding ground width of the array is $1.58\lambda_0$. The antenna element performance is maintained even with the sharing shorted patches. Besides, a conventional 1-to-4 Wilkinson power divider acts as a feeding network as depicted in Fig. 9(b).

The influence of different widths w_1 of the quarter-wavelength impedance transformer on the impedance bandwidth is shown in Fig. 10 when the other dimensions are kept the same as those in Fig. 1. The bandwidth increases when width w_1 decreases, but when width w_1 is less than 2.66 mm, the matching at the higher frequency worsens. Hence, when width w_1 is selected as 2.66 mm, the simulated impedance bandwidth reaches 22.74% (4.48–5.63 GHz) for $|S_{11}| \leq -10$ dB. Compared with the single element with impedance bandwidth of 18.01%, the impedance bandwidth of the array is improved by exciting a new resonant due to the compact array arrangement.

IV. Experimental Results and Discussion

The 2 × 2 array prototype is fabricated and measured as depicted in Fig. 11 to validate the proposed design.

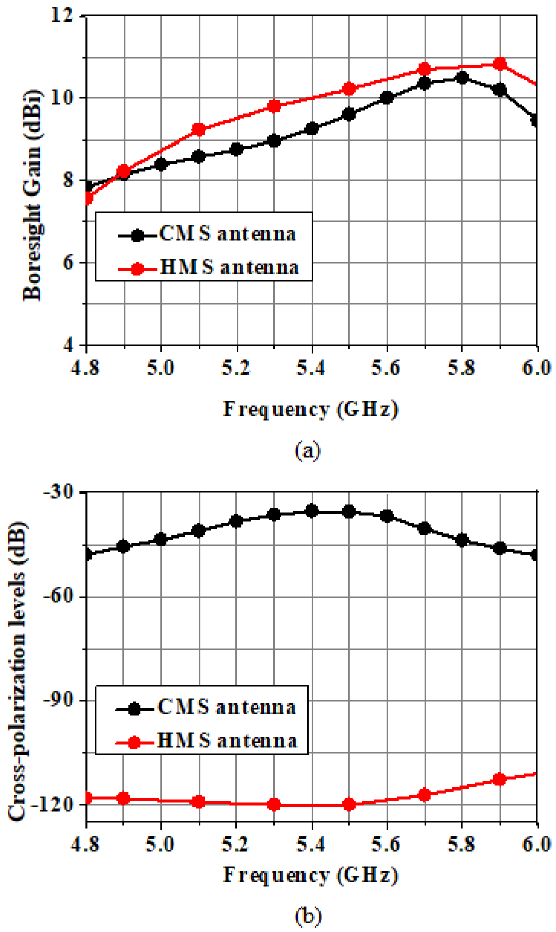

Fig. 8. Simulated (a) boresight gain and (b) cross-polarization levels at boresight of the CMS antenna and HMS antenna.

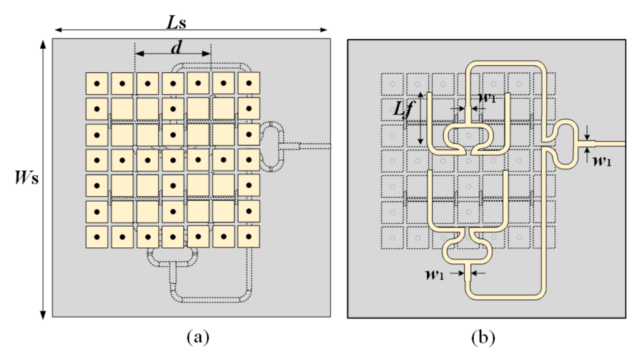

Fig. 9. Configuration of the 2 × 2 antenna array. (a) Top view. (b) Back view. ($Ws = Ls = 95$, $d = 30$, $Lf = 21$, and $w_1 = 2.66$. Unit: mm).

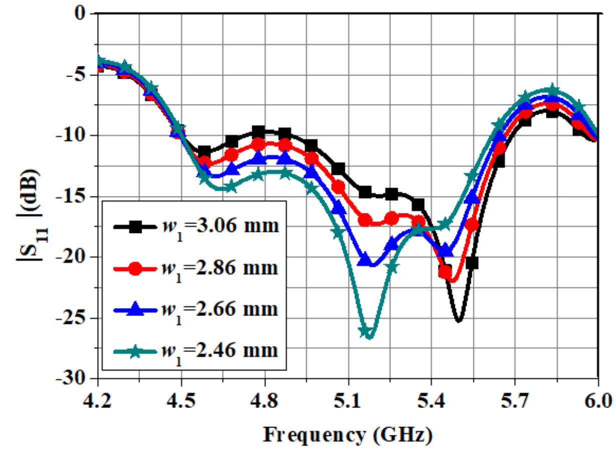

Fig. 10. Simulated reflection coefficients for different widths.

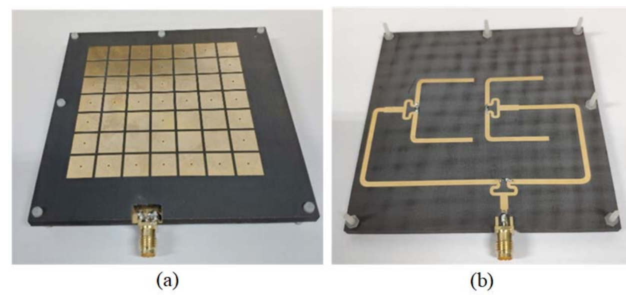

Fig. 11. Photographs of the fabricated prototype. (a) Top view. (b) Back view.

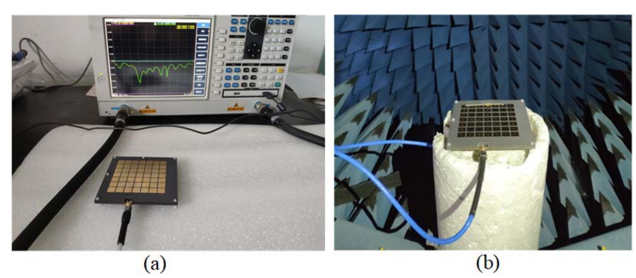

Fig. 12. Antenna measurement setups. (a) Agilent PNA E3861A vector network analyzer for measuring S-parameter. (b) SATIMO antenna measurement system for measuring radiation characteristics.

Nylon bolts with a 2 mm diameter are used to fix the upper and lower substrates. The reflection coefficients and radiation of the prototype are measured using an Agilent PNA E8361A vector network analyzer and a SATIMO antenna measurement system, respectively, as shown in Fig. 12. Besides, Figs. 13–15 compare the simulated and measured results.

From Fig. 13, it can be seen that the measured S-parameters agree well with the simulated results, both with three resonant points. The measured −10 dB impedance band is 4.41–5.85 GHz (28%), 290 MHz wider than that predicted by the simulation, and the three dips slightly move to the higher frequencies. The discrepancy may be caused by fabrication and assembly error. In addition, to show the effects of the gap between the upper and lower substrates on reflection coefficient, the simulated S-parameters for varying gaps are given in Fig. 16. As can be seen, the three resonances move to the higher frequencies as the gap increases.

Fig. 14 compares the simulated and measured radiation efficiencies and gain. Within the band of 4.6–5.6 GHz, the simulated/measured efficiencies are greater than 80%/72%, and the boresight gains are higher than 10.4 dBi/9.7 dBi, respectively. The measured results are lower than the simulated ones, which may be caused by the machining error and metal loss. From Fig. 14, it can be seen that over the 4.6–5.6 GHz, the simulated gain reaches up to 13.4 dBi with a variation of 2.8 dB, while the measured one is up to 12.1 dBi with a variation of 2.4 dB. Besides, a measured average gain of 10.9 dBi is obtained by calculating the arithmetic mean of

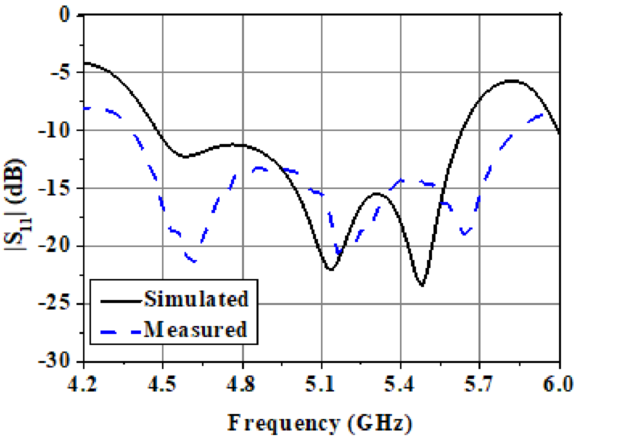

Fig. 13. Simulated and measured reflection coefficients of the antenna array.

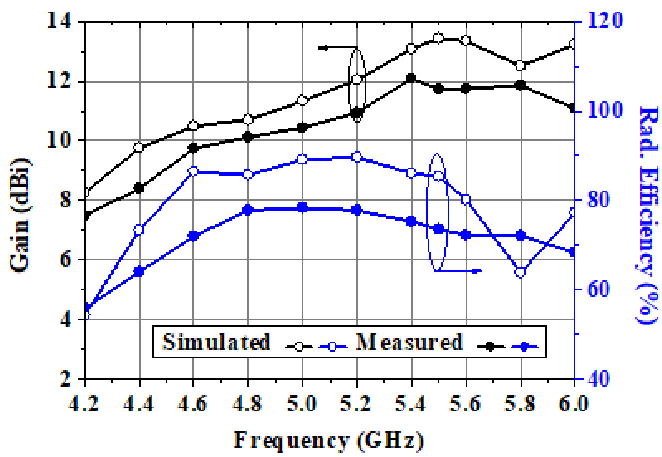

Fig. 14. Simulated and measured radiation efficiencies and boresight gains of the antenna array.

boresight gains at the frequencies with an interval of 100 MHz across the measured band of 4.4−5.9 GHz.

Fig. 15 shows the simulated and measured normalized radiation patterns at 4.6, 5.1, and 5.6 GHz, which are normalized with respect to the peak gain at respective frequency. The simulation and measurement are in excellent agreement. Also, the maximum radiation of the antenna array is in the desired boresight direction across the operating band. Due to the surface waves being depressed by the shorting pins, and the symmetrical feeding design, the measured cross-polarization levels at boresight are less than −30 dB over the operating band.

To highlight the merits of the proposed antenna, the size and performance comparison with some previously reported MS antennas [17], [23]–[27] is carried out and listed in Table I. Obviously, the HMS antenna array is more compact than those in [17], [22], and [23] while still maintaining a wider or comparable bandwidth. An extremely compact MS antenna array was designed based on substrate integrated waveguide (SIW), but the impedance bandwidth is only 5.3% [24]. Compared with the MS antennas in [25] and [26], the proposed HMS antenna element has a smaller size, lower cross-polarization level, and a comparable gain with similar thickness. Besides, in comparison with the MS antenna in [27], the profile of the proposed HMS antenna

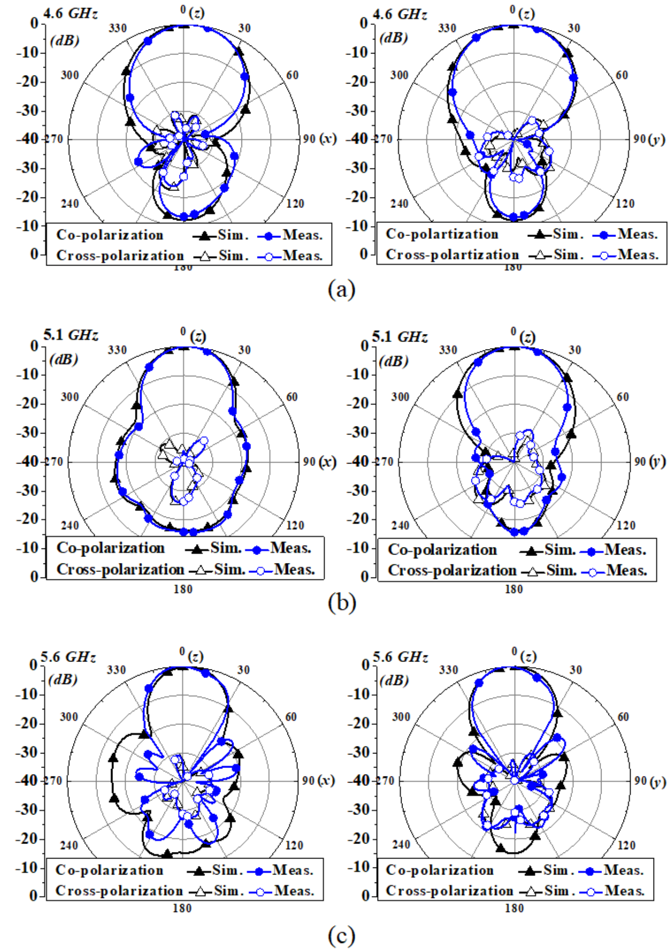

Fig. 15. Simulated and measured radiation patterns at selected frequencies of the antenna array in the *xz* and *yz* planes. (a) 4.6 GHz. (b) 5.1 GHz. (c) 5.6 GHz.

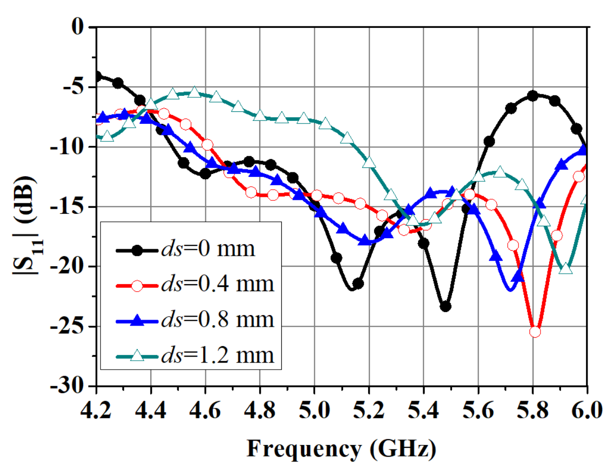

Fig. 16. Simulated reflection coefficients for different gaps between the upper and lower substrates.

has been significantly reduced with a comparable size and gain.

In short, the proposed HMS antenna has achieved desired performance enhancement. In particular, the interelement spacing has been reduced by more than 22% compared to [17], [22], and [23], and the grating lobes of the HMS antenna array are lower due to the smaller interelement spacing.

TABLE I
FIGURE-OF-MERITS COMPARISON WITH SOME PREVIOUSLY REPORTED MS ANTENNAS

Reference	Total Size	IBW (GHz)	Number of Elements	Antenna Design	Boresight Gain (dBi)	XP (dB)	CCD
[17]	$1.78\lambda_0\times1.78\lambda_0\times0.07\lambda_0$	4.61-6.24 (31%)	4	Simple	11.2~14.1	<−30	$0.77\lambda_0/1.42\lambda g$
[22]	$6.72\lambda_0\times7.08\lambda_0\times0.13\lambda_0$	56.3-65.7 (15.4%)	64	Complex	21.5~24.2	<−20	$0.84\lambda_0/2.04\lambda g$
[23]	$3.05\lambda_0\times4.35\lambda_0\times0.16\lambda_0$	26.6-38.7 (37%)	4	Simple	9.1~13.8	<−24	$0.76\lambda_0/1.13\lambda g$
[24]	$0.97\lambda_0\times0.97\lambda_0\times0.07\lambda_0$	5.69-6.0 (5.3%)	4	Complex	7.2~10.75	<−25	$0.41\lambda_0/0.86\lambda g$
[25]	$1.13\lambda_0\times1.13\lambda_0\times0.09\lambda_0$	4.08-6.38 (44%)	1	Complex	7.9~11.6	<−15	—
[26]	$1.01\lambda_0\times1.61\lambda_0\times0.08\lambda_0$	11.9-18.2 (40%)	1	Simple	7~10.4	<−18	—
[27]	$1.02\lambda_0\times1.02\lambda_0\times0.11\lambda_0$	3.95-6.23 (45%)	1	Complex	8.5~11.6	<−25	—
Element*	$1.03\lambda_0\times1.03\lambda_0\times0.07\lambda_0$	4.96–5.94 (18.1%)	1	Simple	8.4~10.9	<−30	—
2×2 Array	$1.63\lambda_0\times1.63\lambda_0\times0.07\lambda_0$	4.41-5.85 (28%)	4	Simple	8.3~12.1	<−30	$0.51\lambda_0/0.94\lambda g$

*By simulation. Element is the proposed hybrid metasurface antenna element. IBW: −10-dB impedance bandwidth. XP: cross-polarization. CCD: center-to-center distance.

V. CONCLUSION

An HMS-based low-profile wideband antenna has been proposed for compact high-performance array design. A wide impedance band of the HMS antenna has been achieved by exciting dual resonance modes simultaneously with broadside radiation. Compared with the CMS antenna, the cross-polarization levels and gain of the HMS antenna have been improved due to the shorting pins depressing the surface waves. Based on the HMS antenna, a compact 2×2 array has been designed and fabricated. The HMS array has achieved a bandwidth of 28% with an average gain of 10.9 dBi, radiation efficiency above 68%, and cross-polarization level below -30 dB. The HMS antenna array can be an excellent candidate for 5G sub-6 GHz and WiFi systems due to its compact size, satisfactory performance, and easy integration with a planar structure.

ACKNOWLEDGMENT

The authors would like to thank Dr. W. Liu and Dr. F. Han Lin of National University of Singapore, for their help in the antenna analysis and simulation.

REFERENCES

[1] M.-Y. Li *et al.*, "Eight-port orthogonally dual-polarized antenna array for 5G smartphone applications," *IEEE Trans. Antennas Propag.*, vol. 64, no. 9, pp. 3820–3830, Sep. 2016.
[2] B. Feng, K. L. Chung, J. Lai, and Q. Zeng, "A conformal magneto-electric dipole antenna with wide H-plane and band-notch radiation characteristics for sub-6-GHZ 5G base-station," *IEEE Access*, vol. 7, pp. 17469–17479, 2019.
[3] F. Liu, J. Guo, L. Zhao, and Y. Yin, "A meta-surface decoupling method for two linear polarized antenna array in sub-6 GHz base station applications," *IEEE Access*, vol. 7, pp. 2759–2768, 2019.
[4] J. Hu, Z.-C. Hao, and W. Hong, "Design of a wideband quad-polarization reconfigurable patch antenna array using a stacked structure," *IEEE Trans. Antenna Propag.*, vol. 65, no. 6, pp. 3014–3023, Jun. 2017.
[5] S.-H. Wi, Y.-S. Lee, and J.-G. Yook, "Wideband microstrip patch antenna with U-shaped parasitic elements," *IEEE Trans. Antennas Propag.*, vol. 55, no. 4, pp. 1196–1199, Apr. 2007.
[6] S. L. S. Yang and K.-M. Luk, "A wideband l-probes fed circularly-polarized reconfigurable microstrip patch antenna," *IEEE Trans. Antennas Propag.*, vol. 56, no. 2, pp. 581–584, Feb. 2008.
[7] D. Sun and L. You, "A broadband impedance matching method for proximity-coupled microstrip antenna," *IEEE Trans. Antennas Propag.*, vol. 58, no. 4, pp. 1392–1397, Apr. 2010.
[8] J. Hu, G. Q. Luo, and Z.-C. Hao, "A wideband quad-polarization reconfigurable metasurface antenna," *IEEE Access*, vol. 6, pp. 6130–6137, 2018.
[9] S.-X. Ta and I. Park, "Low-profile broadband circularly polarized patch antenna using metasurface," *IEEE Trans. Antennas Propag.*, vol. 63, no. 12, pp. 5929–5934, Dec. 2015.
[10] T. Yue, Z. H. Jiang, and D. H. Werner, "Compact, wideband antennas enabled by interdigitated capacitor-loaded metasurfaces," *IEEE Trans. Antennas Propag.*, vol. 64, no. 5, pp. 1595–1606, May 2016.
[11] S. S. S. Nasser, W. Liu, and Z. N. Chen, "Wide bandwidth and enhanced gain of a low-profile dipole antenna achieved by integrated suspended metasurface," *IEEE Trans. Antennas Propag.*, vol. 66, no. 3, pp. 1540–1544, Mar. 2018.
[12] C. L. Holloway, E. F. Kuester, J. A. Gordon, and J. O'Hara, J. Booth, and D. R. Smith, "An overview of the theory and applications of metasurfaces: The two-dimensional equivalents of metamaterials," *IEEE Antennas Propag. Mag.*, vol. 54, no. 2, pp. 10–35, Apr. 2012.
[13] H. L. Zhu, S. W. Cheung, K. L. Chung, and T. I. Yuk, "Linear-to-circular polarization conversion using metasurface," *IEEE Trans. Antennas Propag.*, vol. 61, no. 9, pp. 4615–4623, Sep. 2013.
[14] K. Konstantinidis, A. P. Feresidis, and P. S. Hall, "Broadband sub-wavelength profile high-gain antennas based on multi-layer metasurfaces," *IEEE Trans. Antennas Propag.*, vol. 63, no. 1, pp. 423–427, Jan. 2015.
[15] W. Liu, Z. N. Chen, and X. Qing, "Metamaterial-based low-profile broadband mushroom antenna," *IEEE Trans. Antennas Propag.*, vol. 62, no. 3, pp. 1165–1172, Mar. 2014.
[16] W. Liu, Z. N. Chen, and X. Qing, "Metamaterial-based low-profile broadband aperture-coupled grid-slotted patch antenna," *IEEE Trans. Antennas Propag.*, vol. 63, no. 7, pp. 3325–3329, Jul. 2015.
[17] F. H. Lin and Z. N. Chen, "Low-profile wideband metasurface antennas using characteristic mode analysis," *IEEE Trans. Antennas Propag.*, vol. 65, no. 4, pp. 1706–1713, Apr. 2017.
[18] T. Li and Z. N. Chen, "A dual-band metasurface antenna using characteristic mode analysis," *IEEE Trans. Antennas Propag.*, vol. 66, no. 10, pp. 5620–5624, Oct. 2018.
[19] P. Deo, A. Mehta, D. Mirshekar-Syahkal, P. J. Massey, and H. Nakano, "Thickness reduction and performance enhancement of steerable square loop antenna using hybrid high impedance surface," *IEEE Trans. Antennas Propag.*, vol. 58, no. 5, pp. 1477–1485, May 2010.
[20] A. Pal, A. Mehta, D. Mirshekar-Syahkal, and H. Nakano, "2×2 phased array consisting of square loop antennas for high gain wide angle scanning with low grating lobes," *IEEE Trans. Antennas Propag.*, vol. 65, no. 2, pp. 576–583, Feb. 2017.
[21] *Computer Simulation Technology*. CST Microwave Studio. Accessed: 2018. [Online]. Available: http://www.cst.com/Content/Products/MWS/Overview.Aspx
[22] W. Liu, Z. N. Chen, and X. Qing, "60-GHz thin broadband high-gain LTCC metamaterial-mushroom antenna array," *IEEE Trans. Antennas Propag.*, vol. 62, no. 9, pp. 4592–4601, Sep. 2014.
[23] T. Li and Z. N. Chen, "Wideband substrate-integrated waveguide-fed endfire metasurface antenna array," *IEEE Trans. Antennas Propag.*, vol. 66, no. 12, pp. 7032–7040, Dec. 2018.
[24] W. Yang, S. Chen, W. Che, Q. Xue, and Q. Meng, "Compact high-gain metasurface antenna arrays based on higher-mode SIW cavities," *IEEE Trans. Antennas Propag.*, vol. 66, no. 9, pp. 4918–4923, Sep. 2018.
[25] Z.-Z. Yang, F. Liang, Y. Yi, D. Zhao, and B.-Z. Wang, "Metasurface-based wideband, low-profile, and high-gain antenna," *IET Microw. Antennas Propag.*, vol. 13, no. 4, pp. 436–441, Mar. 2019.

[26] Y. Cao *et al.*, "Broadband and high-gain microstrip patch antenna loaded with parasitic mushroom-type structure," *IEEE Antennas Wireless Propag. Lett.*, vol. 18, no. 7, pp. 1405–1409, Jul. 2019.
[27] F. H. Lin and Z. N. Chen, "Truncated impedance sheet model for low-profile broadband nonresonant-cell metasurface antennas using characteristic mode analysis," *IEEE Trans. Antennas Propag.*, vol. 66, no. 10, pp. 5043–5051, Oct. 2018.

Nian-Sheng Nie (S'19) was born in Yunnan, China, 1994. He received the B.S. degree in electronic information science and technology from the University of Electronic Science and Technology of China (UESTC), Chengdu, China, in 2017, where he is currently pursuing the M.S. degree in radio physics.

His current research interests include antenna theory and engineering, phased arrays, and metasurface antennas.

Xue-Song Yang (M'12) received the B.Eng. degree in applied electronic technology from the Huazhong University of Science and Technology (HUST), Wuhan, China, in 1991, and the Ph.D. degree in radio physics from the University of Electronic Science and Technology of China (UESTC), Chengdu, China, in 2006.

She joined UESTC in 2002, where she is currently a Full Professor. From January 2007 to July 2008, she was a Senior Research Associate and then a Research Fellow with the City University of Hong Kong (CITYU), Hong Kong. From December 2009 to December 2010, she was a Visiting Scholar with the University of Southern California (USC), Los Angeles, CA, USA. From July 2014 to August 2014, she was a Visiting Associate Professor with CITYU. From December 2017 to December 2018, she was a Visiting Scholar with the National University of Singapore (NUS), Singapore. Her current research interests include MIMO antennas, reconfigurable antennas, metasurface antennas, wireless energy transmission, and wireless communications channel modeling.

Zhi Ning Chen (M'99–SM'05–F'07) received the B.Eng., M.Eng., and Ph.D. degrees in electrical engineering from the Institute of Communications Engineering (ICE), Nanjing, China, in 1985, 1988, and 1993, respectively, and the second Ph.D. degree from the University of Tsukuba, Tsukuba, Japan, in 2003.

From 1988 to 1995, he was a Lecturer and later a Professor with ICE. He was a Post-Doctoral Fellow and later an Associate Professor with Southeast University, Nanjing. From 1995 to 1997, he was a Research Assistant and later a Research Fellow with the City University of Hong Kong, Hong Kong. In 1997, he was awarded the Japan Society for the Promotion of Science (JSPS) Fellowship to conduct his research at the University of Tsukuba. From 1999 to 2016, he was a Principal Scientist with the Institute for Infocomm Research (I^2R), Singapore, where he was the Head/Manager of the RF and Optical Department, and a Technical Advisor. In 2001 and 2004, he visited the University of Tsukuba twice under the JSPS Fellowship Program (Senior Fellow). In 2004, he joined the IBM T. J. Watson Research Center, Yorktown Heights, NY, USA, as an Academic Visitor. In 2012, he joined the Department of Electrical and Computer Engineering, National University of Singapore, Singapore, as a tenured Full Professor, and is currently the Program Director (Industry). In 2013, he visited the "Laboratoire des SignauxetSystèmes," UMR8506 CNRS-Supelec-University Paris Sud, Gif-sur-Yvette, France, as a Senior DIGITEO Guest Scientist. In 2015, he visited the Center for Northeast Asian Studies, Tohoku University, Sendai, Japan, as a Senior Visiting Professor. He is holding/held the concurrent guest professorships with Southeast University, Nanjing University, Nanjing, Tsinghua University, Beijing, China, Shanghai Jiao Tong University, Shanghai, China, Tongji University, Shanghai, the University of Science and Technology of China, Hefei, China, Fudan University, Shanghai, Dalian Maritime University, Dalian, Chiba University, Chiba, Japan, the National Taiwan University of Science and Technology, Taipei, Taiwan, the South China University of Technology, Guangzhou, China, Shanghai University, Shanghai, the Beijing University of Posts and Telecommunications, Beijing, Yunnan University, Kunming, China, the Beijing Institute of Technology, Beijing, and the City University of Hong Kong. He was a Changjiang Chair Professor with Southeast University. He is currently serving as a member of the State Key Laboratory of Millimeter-Waves, Southeast University, and also with the State Key Laboratory of Tera-Hertz and Millimeter-Waves, City University of Hong Kong. He has provided 11 local and overseas telecommunication and IT MNCs and SMEs with the technical consultancy service as a Technical Advisor, a Guest Professor, and a Chief Scientist. He has authored more than 650 academic articles and five books entitled *Broadband Planar Antennas* (Wiley 2005), *UWB Wireless Communication* (Wiley 2006), *Antennas for Portable Devices* (Wiley 2007), *Antennas for Base Stations in Wireless Communications* (McGraw-Hill 2009), and *Handbook of Antenna Technologies* with 76 chapters (by Springer References in 2016 as an Editor-in-Chief). He has also contributed the chapters to the books entitled *Developments in Antenna Analysis and Design*(IET 2018), *UWB Antennas and Propagation for Communications, Radar, and Imaging* (Wiley 2006), *Antenna Engineering Handbook* (McGraw-Hill 2007), *Microstrip and Printed Antennas* (Wiley 2010), and *Electromagnetics of Body Area Networks* (Wiley 2016). He holds 32 granted/filed patents and completed more than 38 technology licensed deals with industry. His current research interests include developing small and wideband/ultra-wideband antennas, wearable/implanted medical antennas, package antennas, near-field antennas/coils, 3-D integrated LTCC arrays, microwave lens antennas, microwave metamaterial-metasurface antennas for communications, sensing, imaging systems, and the translational research of metasurfaces into antenna engineering.

Dr. Chen was a recipient of the International Symposium on Antennas and Propagation Best Paper Award in 2010, the CST University Publication Awards in 2008 and 2015, the ASEAN Outstanding Engineering Achievement Award in 2013, the Institution of Engineers Singapore Prestigious Engineering Achievement Awards in 2006, 2013 (two awards), and 2014, the I^2R Quarterly Best Paper Award in 2004, the IEEE iWAT Best Poster Award in 2005, several technology achievement awards from China from 1990 to 1997, and more than 21 academic awards by the students under his supervision. He was elevated as a fellow of the Academy of Engineering, Singapore, in 2019. He has been serving as the Vice-President and a Distinguished Lecturer of the IEEE Council on RFID, since 2015. He served as an Associate Editor for the IEEE TRANSACTIONS ON ANTENNAS AND PROPAGATION and a Distinguished Lecturer of the IEEE Antennas and Propagation Society. He is the Founding General Chair of the International Workshop on Antenna Technology (iWAT), in 2005, the International Symposium on InfoComm & Mechatronics Technology in Bio-Medical and Healthcare Application (IS 3Tin3A), in 2010, the International Microwave Forum (IMWF), in 2010, and the Asia–Pacific Conference on Antennas and Propagation (APCAP), in 2012. He has been also involved in many international events as the General Chair, the Chair, and a member of technical program committees and international advisory committees. He has been invited to deliver more than 90 keynote/plenary/invited speeches at international academic and industry events.

Bing-Zhong Wang (M'06–SM'16) received the Ph.D. degree in electronic engineering from the University of Electronic Science and Technology of China (UESTC), Chengdu, China, in 1988.

He joined UESTC in 1984 and is currently a Professor. He has been a Visiting Scholar with the University of Wisconsin–Milwaukee, Milwaukee, WI, USA, a Research Fellow with the City University of Hong Kong, Hong Kong, and a Visiting Professor with the Electromagnetic Communication Laboratory, Pennsylvania State University, University Park, PA, USA. His current research interests include computational electromagnetics, antenna theory and technique, and time-reversed electromagnetics.